

## **Section 7**

**Global and regional climate models,  
sensitivity and impact experiments,  
response to external forcing**



## Simulating High-Resolution Atlantic Tropical Cyclones using GEM: Part II

Louis-Philippe Caron<sup>1</sup> Colin G. Jones<sup>2</sup> Katja Winger<sup>1</sup>

<sup>1</sup> CRCMD Network, Université du Québec à Montréal

<sup>2</sup> Rossby Center, Swedish Meteorological and Hydrological Institute

emails: lpcaron@sca.uqam.ca, jones.colin@smhi.se, katja.winger@ec.gc.ca

In a previous paper (Caron et al., 2008), we discussed Atlantic tropical cyclone (TC) activity over a 26-year period as simulated by the Global Environmental Multiscale (GEM) model (Zadra et al., 2008) using observed sea surface temperatures. GEM has the ability to run in variable resolution so that the region of interest can be integrated at high-resolution while the rest of the globe is run at lower resolution, typical of today's global climate models (GCMs). For this experiment, the high-resolution region ( $0.3^\circ$ ) was chosen to extend from the Eastern Pacific to the Arabian Sea in order to cover the whole tropical Atlantic as well as the entire Sahel region where the African Easterly waves, precursors of a large portion of Atlantic TCs, are formed (figure 1).

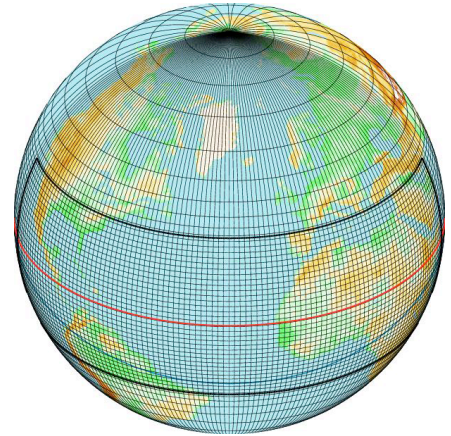


Figure 1: Variable-resolution grid used in this study.

We showed that GEM managed to capture TC intra-annual variability, with maximum activity in September, yet produced too many storms overall with respect to observations for the given period. Also, the storms produced by GEM had the tendency to be too weak in comparison with their observed counterpart: based on the maximum wind speed produced during their entire lifetime, no storm stronger than category 1 on the Saffir-Simpson scale was detected ( $\sim 145 \text{ km h}^{-1}$ ). Here, we extend the study period to 2006 and follow up on these issues.

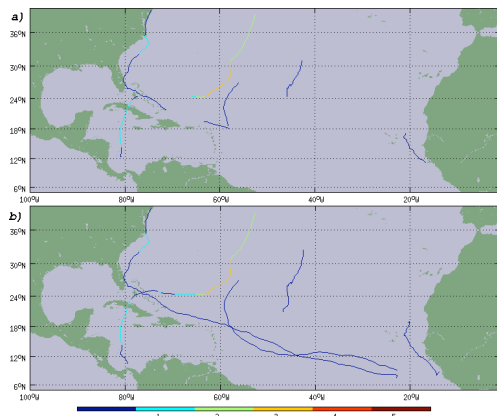


Figure 2: Same hurricane season as seen by a) the previous tracking procedure and b) the current tracking procedure. The scale represents TC intensities as measured by the Saffir-Simpson scale based on minimum central pressure.

When tracking TCs, we followed the scheme suggested by Walsh et al. (2007). As such, a storm is detected if it fulfills the following conditions for a 24h period:

- a minimum pressure in the center.
- surface winds of at least  $17 \text{ m s}^{-1}$  ( $65 \text{ km h}^{-1}$ ) in the vicinity of the center.
- a warm core in the mid- to upper-troposphere.

No standard algorithm yet exists for identifying a warm core, and various definitions have been used in different studies (Walsh et al., 2007). In Caron et al. (2008), a warm core was positively identified if 1) the mean temperature in a  $2^\circ$  radius around the storm center at  $500 \text{ hPa}$  and  $250 \text{ hPa}$  was  $1^\circ\text{C}$  greater than the temperature at a  $5^\circ$  radius at the same levels, and 2) the low-level ( $850 \text{ hPa}$ ) wind was higher than the upper-level ( $250 \text{ hPa}$ ) wind. This technique is very efficient for discarding false-positives, but because of its stringent nature, has the disadvantage of double counting the storms that weaken (and therefore are no longer detected) and later re-intensify.

In order to address this issue, we modified the tracking procedure such that it is now performed in multiple steps. The first step has already been described above. The second step consists of running the tracking procedure a second time, but changing the surface wind threshold to  $10 \text{ m s}^{-1}$  as well as ignor-

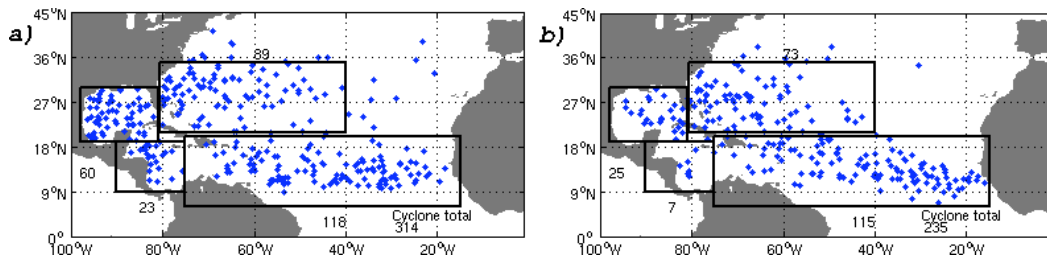


Figure 3: Cyclogenesis location a) observed and b) simulated by GEM for the 1979-2006 period.

ing the difference in temperature in the mid- and upper-troposphere. The comparison between lower and upper wind however, remains. Because more tracks are detected with the second tracking procedure, we then compare both sets of tracks, retaining only those detected using both the more permissive and the more stringent conditions. The different results between the two techniques can be seen in figure 2, which compares the same hurricane season using the previous and current method. The new technique has the added benefit of tracing a storm back to its origin. When compared to observations for the 1979-2006 period (figure 3), TC activity is fairly realistically represented over the entire basin, except in the Gulf of Mexico and the Caribbean Sea, where the number of TCs is too low. The reason for this is currently under investigation.

As mentioned above, based on maximum wind speed, GEM does not simulate storms stronger than category 1 on the Saffir-Simpson scale. However, since there is a relatively good correspondence between the central pressure of a storm and its maximum wind speed, storm intensity can also be estimated using the minimum central pressure. Doing so in our 28-year simulation leads to a different intensity distribution: low-intensity storms are still over-represented, but now storms up to category 4 ( $\sim 945 \text{ hPa}$ ) are present.

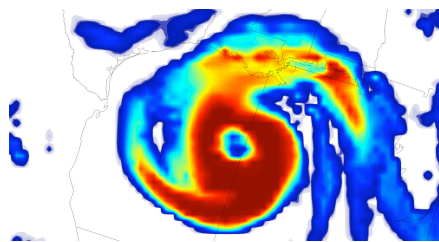


Figure 4: Cloud cover of a strong GEM simulated category 3 (on Saffir-Simpson scale) hurricane in the Gulf of Mexico.

It thus appears that the observed relation between maximum wind speed and minimum central pressure does not hold in GEM. This situation is not unique to GEM and has been observed in other simulations as well (Knutson et al., 2007). The reason for deficiency is not yet clear, but it has been hypothesized that the model misrepresentation of the drag coefficient for very high wind speed could be responsible (Knutson). We are planning to run some tests in that regard where the drag coefficient would be adjusted for hurricane strength wind speed.

Finally, it is worth mentioning that in Caron et al. (2008), we stated that " $0.3^\circ$  appears insufficient resolution for eye development".

This appears to be incorrect, as the most powerful storms simulated do show the presence of an eye. Figure 4 shows a strong category 3 that reached a central pressure of  $\sim 950 \text{ hPa}$  in the Gulf of Mexico. An eye is clearly visible in the cloud cover, with strong ascending motion in the eyewall and descending motion in the eye itself (not shown).

#### References:

- Caron, L.-P., C.G. Jones and K. Winger, 2008: Simulating High-Resolution Atlantic Tropical Cyclones with GEM-Climate. *WGNE Blue Book*, p. 7.05-7.06.
- Knutson, T.R., J.J. Sirutis, S.T. Garner, I.M. Held and R.E. Tuleya, 2007: Simulation of the recent multidecadal increase of Atlantic Hurricane activity using an 18-km-Grid Regional Model. *BAMS*, **88**(10), 1549-1565.
- Walsh, K. J. E., M. Fiorino, C. W. Landsea, and K. L. McInnes, 2007: Objectively Determined Resolution-Dependent Threshold Criteria for the Detection of Tropical Cyclones in Climate Models and Reanalysis. *J. Climate*, **20**, 2307-2314.
- Zadra, A., D. Caya, J. Ct, B. Dugas, C. Jones, R. Laprise, K. Winger and L.-P. Caron, 2008: The next Canadian Regional Climate Model. *Physics in Canada*, **64**, 75-83.

# Sensitivity of methane emissions from wetlands to atmospheric impact in permafrost-covered regions

S.N. Denisov, M.M. Arzhanov, A.V. Eliseev, and I.I. Mokhov  
A.M. Obukhov Institute of Atmospheric Physics RAS, Moscow, Russia  
[denisov@ifaran.ru](mailto:denisov@ifaran.ru)

Model of methane emissions from wetlands [1] is implemented to the dynamic model of thermo- and hydrological processes in soil [2]. Simulations with the combined model are performed for the 21<sup>st</sup> century forced by atmospheric impact from the ensemble of climate models: ECHAM5/MPI-OM, CCCMA-CGCM3, GISS-AOM, IPSL-CM4, and INM CM3.

Simulations are analyzed for the region 65-70°N, 150-160°E in Eastern Siberia. Simulated thaw depths for that region rise by 0.4 m during the 21st century (Fig.1a). On average, simulated methane emissions  $E_{CH_4}$  for that region increase from 1000 mgCH<sub>4</sub>/m<sup>2</sup>/yr for the early 21st century to 2000 mgCH<sub>4</sub>/m<sup>2</sup>/yr to the end of the century (Fig.1b). According to observational estimates [3],  $E_{CH_4}$  equals to 250 mgCH<sub>4</sub>/m<sup>2</sup>/yr for that region. In the climate model of intermediate complexity of the A.M. Obukhov Institute of Atmospheric Physics RAS (IAP RAS CM), methane emissions for the analyzed region increase from 120 to 930 mgCH<sub>4</sub>/m<sup>2</sup>/yr during the 21st century [4]. Estimations of methane emissions obtained for ensemble of models show notable scatter, intermodal differences may be as large as 6000 mgCH<sub>4</sub>/m<sup>2</sup>.

To assess the sensitivity of combined model to input parameters a set of average parameters was constructed for selected site (65°N, 155°E). Simulations of methane emissions are performed for this site with climate forcing from the ensemble of models along with mean model forcing (Fig. 2). Also multiple simulations were made with the input from this “mean” model, when one of input variables is replaced with the same variable from one of the climate models (Table 1). It appears that the combined soil-methane emission model is most sensitive to the temperature at the surface.

This work was supported by the Russian Foundation for Basic Research, by the programs of the Russian Academy of Sciences, and by the Russian President scientific grant.

## References

- [1] Christensen T.R. and Cox P. Response of methane emission from arctic tundra to climatic change: results from a model simulation. *Tellus*, 1995, 47B(3), 301-309.
- [2] Arzhanov M.M., Eliseev A.V., Demchenko P.F., Mokhov I.I., and Khon V.Ch. Simulation of thermal and hydrological regimes of Siberian river watersheds under permafrost conditions from reanalysis data. *Izvestiya, Atmos. Oceanic Phys.*, 2008, 44 (1), 83-89.
- [3] Matthews E., Fung I. Methane emissions from natural wetlands: Global distribution, area and environmental characteristics of sources. *Glob. Biogeochem. Cycles*, 1987, 1, 61-86.
- [4] Eliseev A.V., Mokhov I.I., Arzhanov M.M., Demchenko P.F., Denisov S.N. Interaction of the methane cycle and processes in wetland ecosystems in a climate model of intermediate complexity. *Izvestiya, Atmos. Oceanic Phys.*, 2008, 44 (2), 139-152.

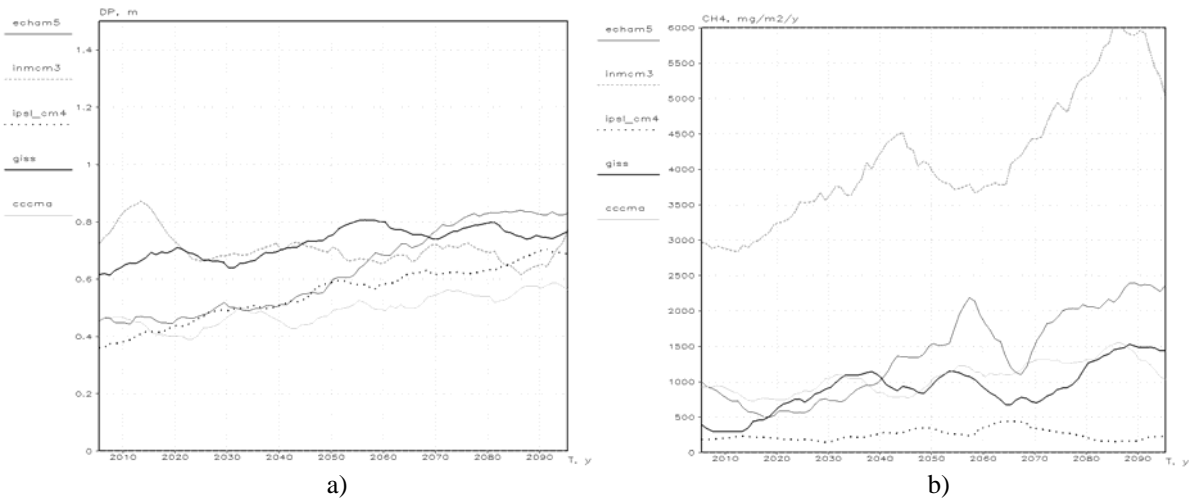


Figure 1: Thaw depths (a) and methane emissions (b) for the Eastern Siberia region (10-year moving average).

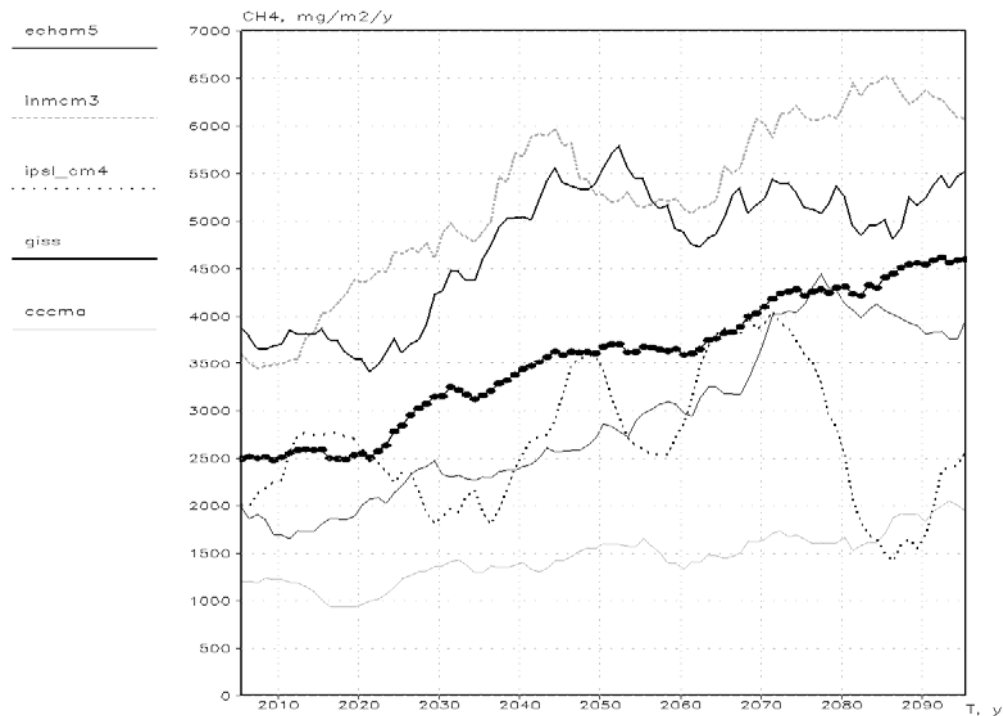


Figure 2: Methane emissions (10-year moving average) for the selected site (line with marks for “mean” model).

	CCCMA- CGCM3	ECHAM5/ MPI-OM	GISS- AOM	INM CM3	IPSL- CM4
Cloudiness	0.7	0.7	0.3	0.5	-5.3
Precipitation	0.4	0.8	-0.4	-0.3	1.9
Humidity	0.6	0.4	1.0	0.5	-5.6
Shortwave radiation	0.4	0.0	0.4	0.1	-0.2
Temperature	28.4	36.2	18.1	29.8	-18.7

Table 1: Ratio of difference between average emissions of methane over 100 years (in %) to difference between the input from the “mean” model and from one of the climatic models (in %).

# Mass balance of the Antarctic ice sheet: conceptual model interpretation

A.V. Malyshkin, I.I. Mokhov

*A.M. Obukhov Institute of Atmospheric Physics RAS, Moscow, Russia*

The present paper's goal is to assess the change of Antarctic ice sheet mass with the use of simple model under projected climate changes. We present conceptual model that takes into account major components of total mass balance: precipitation, melting and ice discharge. We will neglect the components of local mass balance other than precipitation and melting. Precipitation linearly depends on global surface air temperature (SAT)  $T$ .

Melting takes place in the region where surface air temperature (SAT) is positive ( $^{\circ}C$ ). Local rate of melting is assumed to be proportional to SAT similar to [1]. Area  $S$  which positive SAT depends on  $T$ , in particular, linearly. These assumptions allow to obtain the expression for melting:

$$h_m = \frac{\beta r}{v}(d + vT)^2 \quad (1)$$

Speed of ice flow across ocean-continent boundary is supposed to be proportional to third power of average thickness of grounded ice  $H_g$  (by analogy with Glen's law [2, 10]). If ice discharge is proportional to ice thickness at the ocean-continent boundary and ice sheet profile has a shape of parabola [2], then we have

$$\frac{dH_g}{dt} = (a + bT) - \frac{\beta r}{v}(d + vT)^2 - \frac{15}{8}w \left[ 1 - \left( \frac{H_{g0}}{H_g} \right)^2 \right]^{1/2} H_g^4, \quad (2)$$

where  $T_1$  is global average temperature at initial time  $t_0$ ,  $\tau_{cl}$  – time of temperature rise by  $1^{\circ}C$ ,  $H_{g0}$  – average ice thickness at which ice discharge becomes zero. First term in (2) is related with precipitation, second – melting, and third – ice discharge.

In the case of constant ice discharge and if global SAT rises linearly with time, we obtain

$$H_g(t) = H_0 + k_1(t - t_0) + k_2(t - t_0)^2 - k_3(t - t_0)^3, \quad (3)$$

where  $k_1 = a + bT_1 - h_f - \frac{\beta r}{v}(d + vT_1)^2$ ,  $k_2 = \frac{1}{2\tau_{cl}}(b - 2\beta r(d + vT_1))$ ,  $k_3 = \frac{\beta r v}{3\tau_{cl}^2} > 0$ ,  $k_1 = dH_g/dt|_{t=t_0}$ ,  $k_2 = d^2H_g/dt^2|_{t=t_0}$ . Ice sheet may undergo several regimes. Temporal dependence  $H_g(t)$  has minimum and subsequent maximum if the following condition is satisfied

$$b > 2\beta r \left[ d + \left( d^2 + (h_f - a) \frac{v}{\beta r} \right)^{1/2} \right] \quad (4)$$

Denote time of minimum as  $t_1$ , time of inflection –  $t_2$  and time of maximum –  $t_3$  ( $t_1 < t_2 < t_3$ ). Fig. 1 shows straight lines corresponding to  $k_1 = 0$  and  $k_2 = 0$ . Precipitation values of  $100 \text{ mm/yr}$  and  $271 \text{ mm/yr}$  were used as a samples from [3, 4, 5]. These lines constrain four zones which represent qualitatively different cases: 1)  $t_0 < t_1$ :  $k_1 < 0$ ,  $k_2 > 0$ , 2)  $t_1 < t_0 < t_2$ :  $k_1 > 0$ ,  $k_2 > 0$ , 3)  $t_2 < t_0 < t_3$ :  $k_1 > 0$ ,  $k_2 < 0$ , 4)  $t_0 > t_3$ :  $k_1 < 0$ ,  $k_2 < 0$  (Numeration here is the same as in the Fig. 1). When  $t_0 < t_1$  we have decreasing of  $H_g(t)$  at  $t = t_0$  and positive  $k_2$ . Situations 2) and 3) are those which have been noted in some model experiments [5, 6, 7]. According to results of abovementioned simulations, at an initial stage ice sheet grows due to dominating precipitation and shrinks thereafter according to increasing melting. Such behaviour should be attributed to the top part of the  $b - r$  diagram where precipitation is significant. The last case  $t_0 > t_3$  is realized if at initial time melting is enough to overcome the precipitation.

It is noteworthy that numerous ice sheet models have been developed earlier. They span from 0-dimensional [5, 8, 9] (like described one) to thermo-mechanically coupled 3-dimensional models [7, 10, 11]. Proposed model provides a clear analytical interpretation of multiple patterns in behaviour of an ice sheet.

*This study was supported by the RFBR and RAS programs.*

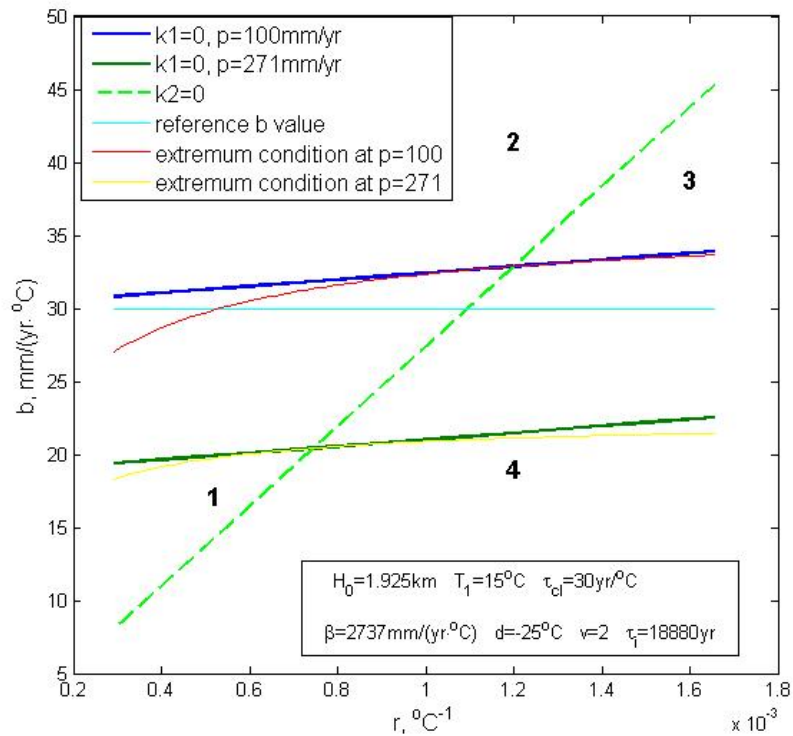


Figure 1: Ice sheet behaviour depending on parameters  $b$  and  $r$

## References

- [1] M. Vizcaino, U. Mikolajewicz, M. Gröger, E. Maier-Reimer, G. Schurgers, A. Winguth (2008) Long-term ice sheet-climate interactions under anthropogenic greenhouse forcing simulated with a complex Earth System Model. *Clim. Dyn.* DOI 10.1007/s00382-008-0369-7.
- [2] W. S. B. Paterson (1994) *Physics of Glaciers*. 3-rd ed., Elsevier Science Ltd., Oxford, Elsevier Science Inc., New York, Elsevier Science Japan, Tokyo, 480 p.
- [3] V. N. Petrov (1975) Atmospheric gain of Antarctic ice sheet, Leningrad, Gidrometeoizdat, 152 p. (in Russian).
- [4] M. Verbitsky (1992) Equilibrium ice sheet scaling in climate modeling. *Clim. Dyn.* 7, 105–110.
- [5] I. I. Mokhov, V. K. Petukhov, I. N. Rusin (1983) Mass exchange sensitivity on the surface of Antarctic ice sheet to climate change. *Meteorol. Hydrol.*, N 11, 52–59.
- [6] U. Micolajewicz, M. Vizcaino, J. Jungclaus, G. Schurgers (2007) Effect of ice-sheet interactions in anthropogenic climate change simulations. *Geophys. Res. Lett.*, 34, L18706.
- [7] P. Huybrechts, J. Wolde (1999) The dynamic response of the Greenland and Antarctic ice sheets to multiple-century climatic warming. *J. Climate*, 2169–2188.
- [8] E. Källén, C. Crafoord, M. Ghil (1979) Free oscillations in a climate model with ice-sheet dynamics. *J. Atmos. Sci.*, 36, 2292–2303.
- [9] V. G. Khodakov (1965) On dependence of total ablation of a glacier surface on air temperature. *Meteorol. Hydrol.*, 7, 48–50.
- [10] R. Greve (1997) A continuum-mechanical formulation for shallow polythermal ice sheets. *Phil. Trans. R. Soc. Lond. A* 355, 921–974.
- [11] M. Verbitsky, B. Saltzman (1997) Modeling the Antarctic ice sheet. *Annals of Glaciology*, 25, 259–267.

## **Cyclonic activity and its total action over extratropical latitudes in Northern Hemisphere from model simulations**

I.I. Mokhov<sup>1</sup>, M.G. Akperov<sup>1</sup>, J.-L. Dufresne<sup>2</sup>, H. Le Treut<sup>2</sup>

<sup>1</sup>Obukhov Institute of Atmospheric Physics RAS, Moscow, Russia

<sup>2</sup>Laboratoire Meteorologie Dynamique du CNRS, Paris, France  
mokhov@ifaran.ru

Changes of cyclonic activity over extratropical latitudes in the Northern Hemisphere (20-80°N) from simulations with the coupled general circulation model (CGCM) are analyzed. Results of the IPSL-CM4 CGCM (Marti et al., 2005) simulations for 1860-2000 with the greenhouse gases concentrations in the atmosphere from observations and for 2001-2100 with the SRES-A2 scenario are used. Cyclonic characteristics (for each 6 hours) were obtained similar to (Akperov et al., 2007; Golitsyn et al., 2007) from model simulations for sea level pressure.

We analyzed probability distributions for extratropical cyclones in dependence on their intensity, size and duration for different seasons. Analysis has been performed also for the atmospheric cyclones action  $S$  as an integral characteristic of their effect. Similar analysis was done by Mokhov (2006a,b) for total action of atmospheric blockings. This value  $S$  has a dimension [energy]x[time]. Action  $S$  of individual climate structure, in particular for cyclonic or anticyclonic vortex, can be defined as follows  $S \sim \int E(t)dt$ , where integration on time  $t$  is performed from 0 to  $\tau$ ,  $\tau$  – vortex life time,  $E$  – vortex energy. Kinetic energy of extratropical (geostrophical) vortex can be expressed via  $(\Delta P)^2$ , where  $\Delta P$  is a pressure difference between centre and periphery of the vortex. Integral action  $S_{\Sigma}$  for ensemble of vortices is defined by the sum of values of action for individual vortices.

Figure 1 shows distributions of the cyclone-days (x4) number as a function of  $\Delta P$  (hPa) from model simulations for the second half of the 20<sup>th</sup> century and also for the first and second half of the 21<sup>st</sup> century. According to Fig. 1 we can expect increase in the number of very strong cyclones.

Analysis of total action for extratropical cyclones from model simulations shows its general decrease in the 21<sup>st</sup> century under global warming. Changes in seasonal values of  $S$  display large interannual and interdecadal variability. Substantial general decrease in the total action of cyclones was noted in winter, while in summer changes in  $S$  are not statistically significant.

This work was supported by the CNRS/RAS Joint Agreement Program, Russian Foundation for Basic Research, Programs of the Russian Academy of Sciences and Russian President Scientific Grant.

### **References**

Akperov M.G., M.Yu. Bardin, E.M. Volodin, G.S. Golitsyn, and I.I. Mokhov, 2007: Probability distributions for cyclones and anticyclones from the NCEP/NCAR reanalysis data and the INM RAS climate model. *Izvestiya, Atmospheric and Oceanic Physics*, **43**, 705–712.

Golitsyn G.S., I.I. Mokhov, M.G. Akperov, and M.Yu. Bardin, 2007: Distribution functions of probabilities of cyclones and anticyclones from 1952 to 2000: An instrument for the determination of global climate variations. *Doklady Earth Sciences*, **413**, 324–326.

Marti O. et al., 2005. The new IPSL climate system model: IPSL-CM4.

<http://dods.ipsl.jussieu.fr/omamce/IPSLCM4/DocIPSLCM4/FILES/DocIPSLCM4.pdf>

Mokhov I.I., 2006a: Action as an integral characteristic for climatic structures: Estimates for atmospheric blockings. *Research Activities in Atmospheric and Oceanic Modelling*, J. Cote (ed.). Geneva: WCRP, WMO TD-No.1347, Section 2, 27-28.

Mokhov I.I., 2006b: Action as an integral characteristic of climatic structures: Estimates for atmospheric blockings. *Doklady Earth Sciences*, **409A**, 925–928.

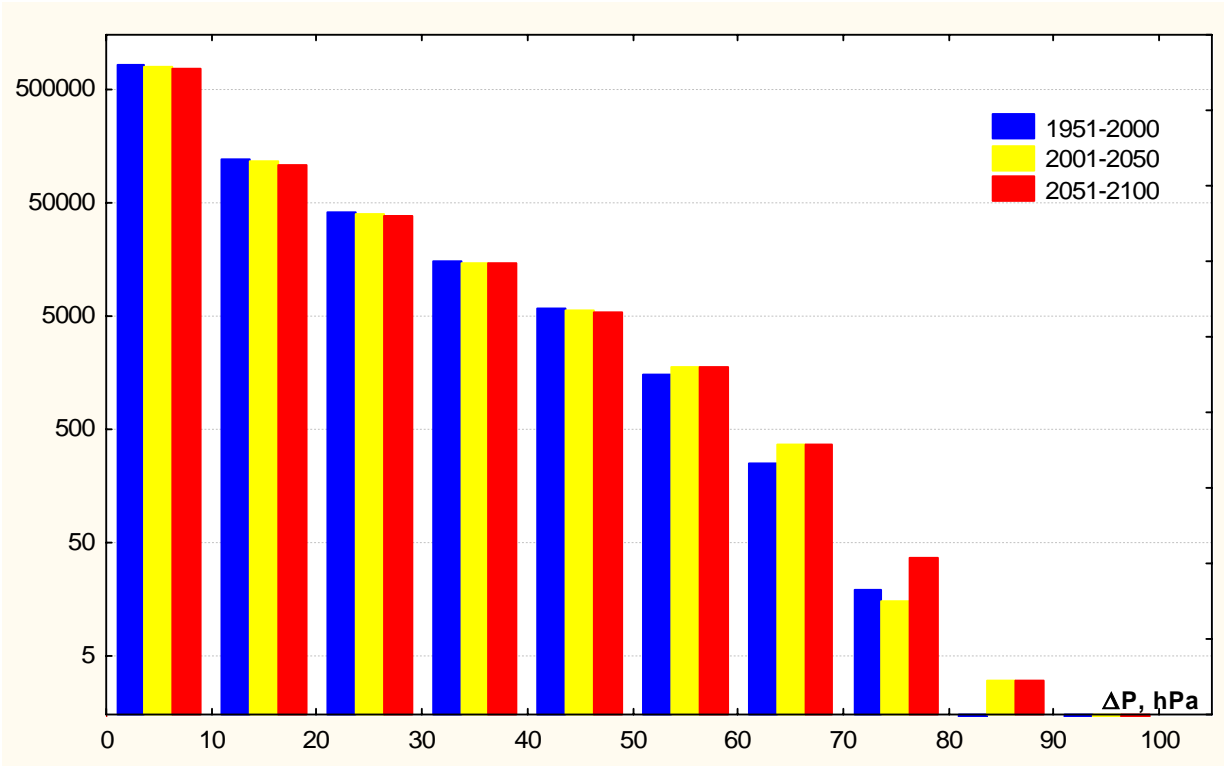


Fig. 1. Distributions of the cyclones number as a function of  $\Delta P$  (hPa) from model simulations for the second half of the 20<sup>th</sup> century and also for the first and second half of the 21<sup>st</sup> century.

# SEASONAL CLIMATE MODEL WITH THERMOHALINE CIRCULATION DESCRIPTION

V.P. Parkhomenko

Computing Centre of the Russia Academy of Sciences

Vavilov Str. 40 Moscow 119967 Russian Federation

E-mail: [parhom@ccas.ru](mailto:parhom@ccas.ru)

C-GOLDSTEIN climate model [1] is used for numerical experiments, but seasonal incoming solar radiation distribution is taking into account. The ocean model is based on the thermocline (or planetary geostrophic) equations, with the addition of a linear drag term in the horizontal momentum equations. In the resulting frictional geostrophic system, density depends nonlinearly on the local values of temperature and salinity, which obey separate advection-diffusion equations and are also subject to convective adjustment. Model vertical levels are uniformly spaced in the logarithmic coordinate so that the upper layers are thinner, while the horizontal grid is uniform in the longitude and sin of latitude coordinates (giving boxes of equal area in physical space). In the vertical there are 8 density levels on a logarithmically stretched grid with vertical spacing increasing with depth from 140 m to 1120 m. The maximum depth is set to 5 km.

Energy Moisture Balance Model (EMBM) of the atmosphere is used [2]. The prognostic variables are air temperature, and specific humidity at the surface. The EMBM solves a vertically integrated equation for air temperature by balancing incoming and outgoing radiation fluxes, sensible (turbulent) heat exchange with the underlying surface, latent heat release due to precipitation, and a simple one layer parameterization of horizontal transport processes. The corresponding transport equation for specific humidity is forced only by precipitation and by evaporation and sublimation at the underlying surface.

A simple representation of sea-ice thermodynamics is similar to that used in the UVic model [2]. Dynamical equations are solved for compactness, the average height of sea ice and the surface temperature.

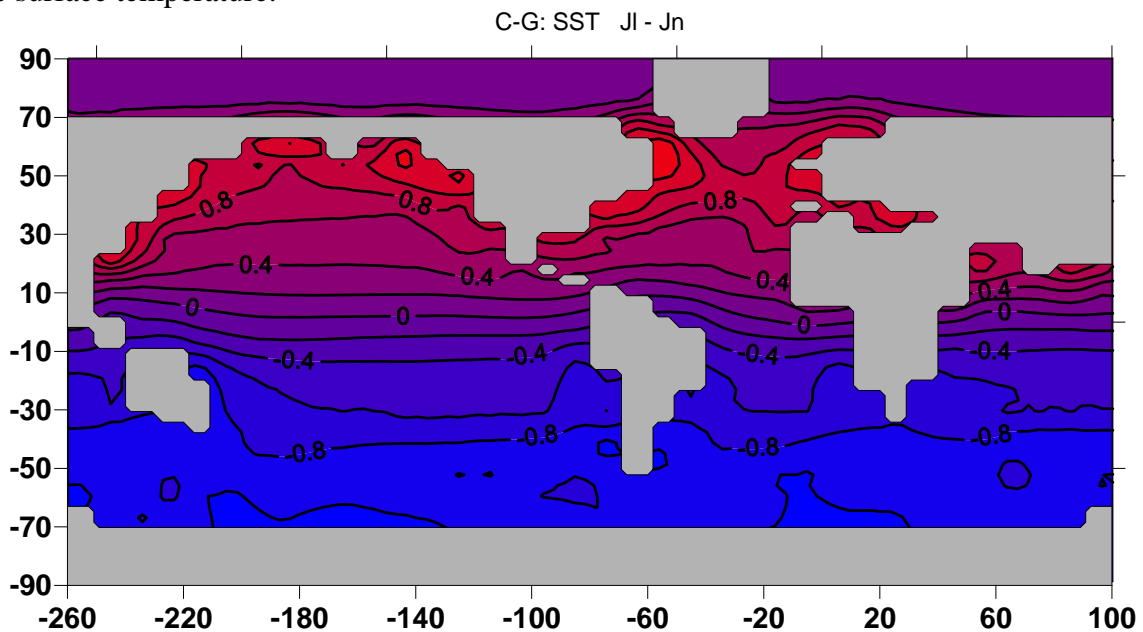


Fig. 1. July and January sea surface temperatures differences. Spinup experiment

Fig. 1 demonstrates July and January sea surface temperatures differences as a result of 2000 years run to obtain a near-equilibrium climate state.

Stable plastic pollution ocean zone is spreaded from California to Japan (Fig. 2) in the Pacific ocean north part [3]. It is possible, that plastic pollution leads to high heating of ocean surface, limiting solar radiation penetration in the deep layers of the ocean. It can cause great water evaporation and possible climate changes. Numerical experiments with climate model under corresponding assumptions show sea surface temperature decreasing in the pollution domain up to 1.8 degrees (Fig. 2). Other climate characteristics are changed also.

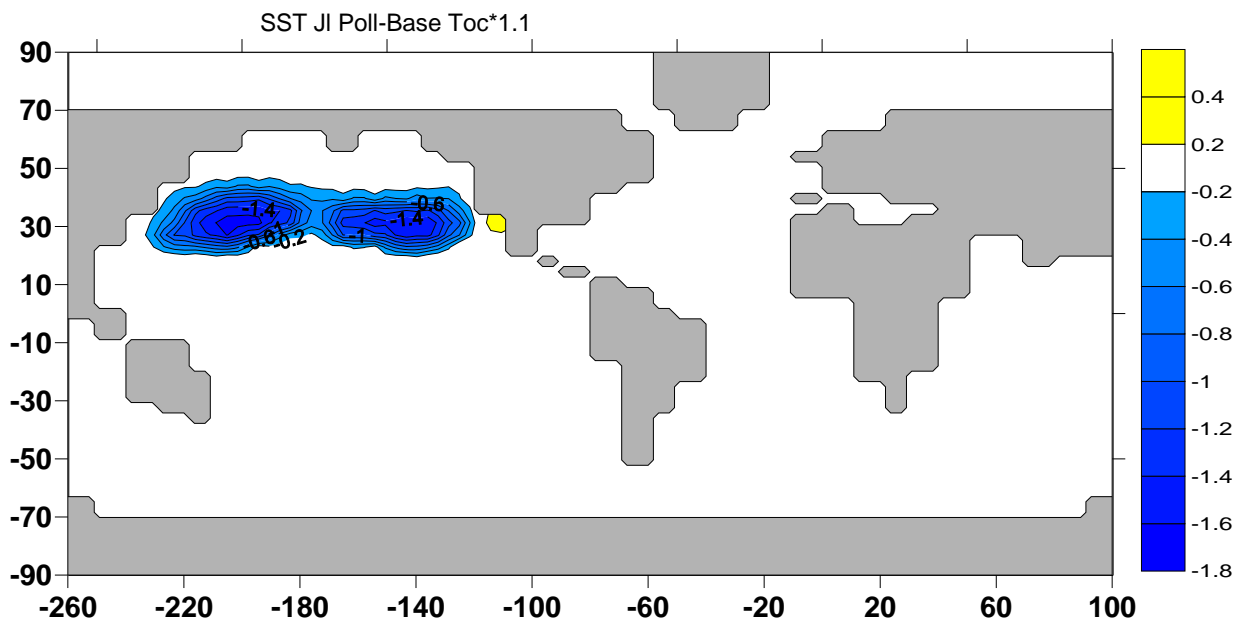


Fig. 2. Sea surface temperature decreasing in the pollution domain in July

### References

1. N.R. Edwards and R. Marsh Uncertainties due to transportparameter sensitivity in an efficient 3-D ocean-climate model. *Clim. Dyn.* 24 (2005).
2. A.J. Weaver, M. Eby, E.C. Wiebe and others. The UVic earth system climate model: Model description, climatology, and applications to past, present and future climates. *Atmos.-Ocean* 39 (2001).
3. S. Casy Best Life Magazine. (2008).